Phys Chem Minerals (2004) 31: 224–231
DOI 10.1007/s00269-003-0364-9

ORIGINAL PAPER

T. Malcherek · A. Bosenick

Structure and phase transition of $CaGe_2O_5$ revisited

Received: 4 June 2003 / Accepted: 23 October 2003

Abstract The structure of $CaGe_2O_5$ between room temperature and 923 K has been determined by X-ray powder diffraction. A continuous phase transition from triclinic $C\bar{1}$ to monoclinic $C2/c$ symmetry at $T_c^\star = 714 \pm 3$ K is observed. The transition is accompanied by a weak heat capacity anomaly. This anomaly and the strain analysis based on the measured lattice parameters indicate a classical second-order phase transition. The order parameter, as measured by the strain component e_{23}, is associated with the displacement of the Ca cation. Electronic structure optimization by density functional methods is used to verify the centric space group of the low-temperature structure of $CaGe_2O_5$.

Keywords Phase transition · Titanite · Sphene · Displacive · Microstrain

Introduction

The structure of calciumdigermanate (CDG) is characterized by a topology common to a wide range of oxide structures of stoichiometry $AMOXO_4$. It consists of parallel chains of *trans* corner sharing MO_6 octahedra, cross-linked by isolated XO_4 tetrahedra. Such a structural topology is realized in the mineral titanite (Taylor and Brown 1976). The room temperature structure of CDG has been described as a triclinically distorted titanite structure, undergoing a reversible transition to the undistorted monoclinic titanite structure type near 773 K (Aust et al. 1976). The purpose of the present paper is to detail the character and mechanism of this phase transition in order to further the understanding of structural instabilities of the underlying titanite framework of parallel octahedral chains and connecting tetrahedra.

In CDG both the octahedrally (M) and the tetrahedrally coordinated (X) sites are occupied by Ge. Ca is sevenfold-coordinated by oxygen atoms but, contrary to titanite, it is not located on a diad axis. Thus, the room-temperature structure is a triclinically distorted titanite structure, isotypic with the amblygonite ($LiAlPO_4F$) structure (Groat et al. 1990). The corresponding silicate, $CaSi_2O_5$, differs in so far that every second Si within the M chains is only five-coordinated by oxygen atoms (Angel et al. 1996). This triclinic form of calcium silicate transforms to the titanite aristotype structure under high-pressure conditions (Angel 1997).

Based on an X-ray single-crystal structure determination, Nevskii et al. (1979) suggested that CDG should be acentric with SG $P1$. Inspection of the atom parameters determined by these authors indicates that the violation of the centre of symmetry would mainly originate from the position of the weakly scattering oxygen atoms. To our knowledge, no conclusive evidence for the acentricity of CDG has so far been reported in the form of its normal structure factor distribution or in the form of characteristic physical properties. In order to overcome this ambiguity, we have verified the validity of the originally suggested centric space group symmetry of Aust et al. (1976) using density functional methods.

Experimental

Powder synthesis of CDG started from pressed pellets of a stoichiometric mixture of GeO_2 and $CaCO_3$. The pellets were decarbonated at 900 °C and then fired at 900 and at 1000 °C for several days.

Differential scanning calorimetry

Heat-capacity measurements between 133 and 923 K were carried out using a power-compensated differential scanning calorimeter

T. Malcherek (✉)
Mineralogisches Institut,
Im Neuenheimer Feld 236,
69120 Heidelberg, Germany
e-mail: tmalch@min.uni-heidelberg.de

A. Bosenick
Institut für Mineralogie,
Westfälische Wilhelms-Universität Münster,
Corrensstr. 24, 48149 Münster, Germany

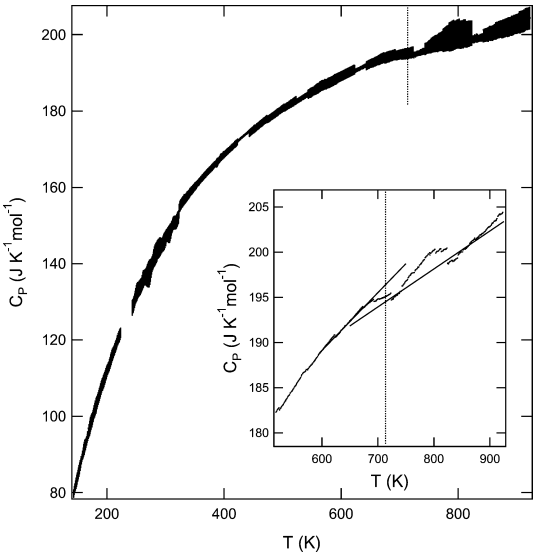

Fig. 1 Heat capacity of CDG as a function of temperature. The measurement uncertainty is shown by *vertical bars* at each temperature. The transition temperature is indicated by a *dotted vertical line*. The *inset* shows c_p close to the phase transition temperature. The *lines* indicate the extrapolated baseline above and below 714 K

(Perkin-Elmer DSC-7, Institut für Geowissenschaften, Kiel). The measurements were performed in two stages: (1) low-temperature c_p measurements between 133 and 348 K and (2) high-temperature c_p measurements between 323 and 923 K. In the low-temperature region, the transition point of cyclohexan (186.09 K) and its melting point at 279.67 K were used for temperature calibration. The measurements were carried out under a constant flow of dried helium gas, keeping the calorimeter block thermostated at 93 ± 1 K. In the high-temperature range, the temperature was calibrated against the melting point of indium (429.75 K) and the phase transition temperature of Li_2SO_4 (851.0 K) (Cammenga et al. 1992). The measurements were made under a constant flow of dried nitrogen gas with the calorimeter block thermostated at 276 ± 1 K. The temperature calibration was checked by measuring the phase-transition temperature of KNO_3 at 401.43 K and the melting point of Zn at 692.67 K. These were found to be accurate within ± 1 K of the literature values (McAdie et al. 1972; Cammenga et al. 1992). A single-crystal synthetic corundum was used for c_p standardization (Ditmars and Douglas 1971). The standard and the sample were placed in cylindrical Au pans, 6 mm in diameter and covered with an Au lid. The c_p measurements were performed using the step-scanning method described by Bosenick et al. (1996). Heat capacities were calculated from three runs (blank run, standard and sample run) (Mraw 1988). The heat capacity shown in Fig. 1 is the average of several scans in the low- and high-temperature range, using heating rates of 20 and 30 K/min^{-1} over temperature intervals between 80 and 100 K.

X-ray powder diffraction

In-situ powder X-ray diffraction measurements were carried out using an Anton Paar HTK1200 furnace on a Philips Xpert diffractometer with monochromatic Cu$K\alpha_1$ radiation. The powder specimen was pressed into an Al_2O_3 sample holder, attached to a sample spinner. Diffraction patterns of CDG were recorded in the range between 16° and 100°2θ using a proportional counter. Various scan speeds were used, with the slowest scans at 0.0019 °s^{-1} and 0.015° step size. Measurements were conducted up to a maximum temperature of 650 °C, heating and cooling through the phase transition in several cycles. Lattice parameters and structural parameters were determined using the Rietveld method as implemented in the GSAS program package (Larson and Von Dreele 1994). The five isotropic thermal parameters of the oxygen atoms in the triclinic phase had to be constrained to the same value in order to obtain positive definite thermal parameters for all atoms. Peak profiles were modelled using profile function #4 which accounts for peak asymmetry due to axial divergence (Finger et al. 1994) and for anisotropic peak broadening (Stephens 1999). Instead of the structural setting used by Aust et al. (1976) with the octahedral chain direction aligned with [101] (Mongiorgi and Riva di Sanseverino 1968), the alternative setting with the chain direction parallel [001] is used here. Lattice parameters and structural parameters at selected temperatures are reported in Tables 1 and 2. Additional lattice parameters close to the critical temperature are shown in Fig. 2.

Table 1 Refined space-group symmetry and lattice parameters of CDG as a function of temperature. Subscript *c* denotes results obtained while cooling the sample

T (K)	SG	a (Å)	b (Å)	c (Å)	$\alpha^{(o)}$	$\beta^{(o)}$	$\gamma^{(o)}$	V (Å^3)	R_p	$R(F^2)$
293	$C\bar{1}$	6.5286(3)	8.7863(4)	6.8616(3)	88.215(1)	113.026(1)	90.988(1)	362.05(3)	0.149	0.065
373	$C\bar{1}$	6.5413(5)	8.7996(7)	6.8718(5)	88.358(2)	113.020(1)	90.895(2)	363.89(4)	0.168	0.089
473	$C\bar{1}$	6.5495(5)	8.8058(7)	6.8758(5)	88.608(2)	113.007(1)	90.749(2)	364.90(5)	0.175	0.092
573	$C\bar{1}$	6.5574(6)	8.8117(8)	6.8794(6)	88.942(2)	112.989(1)	90.555(2)	365.87(6)	0.178	0.100
648_c	$C\bar{1}$	6.5635(6)	8.8160(9)	6.8818(7)	89.342(2)	112.972(1)	90.343(2)	366.60(6)	0.182	0.105
673	$C\bar{1}$	6.5650(6)	8.8168(8)	6.8822(6)	89.472(2)	112.967(1)	90.273(2)	366.76(6)	0.173	0.101
673_c	$C\bar{1}$	6.5658(6)	8.8177(8)	6.8833(6)	89.510(2)	112.963(1)	90.255(2)	366.92(6)	0.181	0.101
703_c	$C\bar{1}$	6.5664(5)	8.8172(6)	6.8825(5)	89.762(2)	112.962(1)	90.119(2)	366.90(5)	0.157	0.091
723	$C\bar{1}$	6.5678(4)	8.8187(5)	6.8833(4)	89.857(2)	112.960(1)	90.072(2)	367.09(4)	0.135	0.073
723_c	$C\bar{1}$	6.5684(4)	8.8193(5)	6.8834(4)	89.866(2)	112.959(1)	90.068(2)	367.16(4)	0.138	0.080
748	$C2/c$	6.5699(4)	8.8212(5)	6.8845(4)	90.0	112.955(1)	90.0	367.39(4)	0.142	0.078
748_c	$C2/c$	6.5702(4)	8.8213(5)	6.8847(4)	90.0	112.956(1)	90.0	367.41(4)	0.140	0.080
773	$C2/c$	6.5720(4)	8.8236(5)	6.8856(4)	90.0	112.952(1)	90.0	367.67(3)	0.138	0.079
773_c	$C2/c$	6.5716(4)	8.8233(5)	6.8854(4)	90.0	112.951(1)	90.0	367.64(4)	0.141	0.077
798	$C2/c$	6.5734(3)	8.8254(5)	6.8865(4)	90.0	112.948(1)	90.0	367.89(3)	0.137	0.080
823	$C2/c$	6.5753(3)	8.8272(5)	6.8876(4)	90.0	112.946(1)	90.0	368.14(3)	0.134	0.075
823_c	$C2/c$	6.5742(3)	8.8260(5)	6.8866(4)	90.0	112.948(1)	90.0	367.96(3)	0.137	0.084
873	$C2/c$	6.5777(3)	8.8302(4)	6.8887(3)	90.0	112.939(1)	90.0	368.48(3)	0.137	0.076
923	$C2/c$	6.5795(3)	8.8321(4)	6.8893(3)	90.0	112.933(7)	90.0	368.70(3)	0.132	0.084

Table 2 Structural parameters of CDG as a function of temperature. Isotropic temperature parameters of the oxygen atoms have been constrained to be identical for all triclinic refinements. A temperature supscript *c* denotes results obtained while cooling the sample

293 K	*x*	*y*	*z*	U_{iso} (Å^2)
Ca	0.9910(7)	0.6694(5)	0.2660(7)	0.0032(15)
Ge(1)	0.9971(4)	0.3142(3)	0.2439(4)	0.0046(9)
Ge(2)	0.0	0.0	0.0	0.0070(13)
Ge(3)	0.0	0.0	0.5	0.0019(12)
O(1)	0.9993(20)	0.9278(12)	0.2523(18)	0.0025(16)
O(2)	0.4047(19)	0.2964(12)	0.9044(18)	0.0025(16)
O(3)	0.8132(18)	0.4505(13)	0.0833(17)	0.0025(16)
O(4)	0.1896(18)	0.4342(12)	0.4297(17)	0.0025(16)
O(5)	0.1188(19)	0.8035(12)	0.6148(18)	0.0025(16)
373 K				
Ca	0.9906(10)	0.6693(7)	0.2645(9)	0.0030(21)
Ge(1)	0.9971(6)	0.3155(4)	0.2438(6)	0.0034(13)
Ge(2)	0.0	0.0	0.0	0.0035(18)
Ge(3)	0.0	0.0	0.5	0.0055(18)
O(1)	0.9977(28)	0.9256(17)	0.2544(25)	0.0048(24)
O(2)	0.4018(26)	0.2937(17)	0.9101(24)	0.0048(24)
O(3)	0.8147(25)	0.4517(18)	0.0859(24)	0.0048(24)
O(4)	0.1823(25)	0.4354(18)	0.4277(24)	0.0048(24)
O(5)	0.1260(27)	0.8002(17)	0.6195(25)	0.0048(24)
473 K				
Ca	0.9937(11)	0.6683(7)	0.2645(10)	0.0052(22)
Ge(1)	0.9979(7)	0.3143(4)	0.2451(6)	0.0025(13)
Ge(2)	0.0	0.0	0.0	0.0012(18)
Ge(3)	0.0	0.0	0.5	0.0047(19)
O(1)	0.0065(30)	0.9260(17)	0.2549(27)	0.0070(25)
O(2)	0.3969(28)	0.2930(18)	0.9042(26)	0.0070(25)
O(3)	0.8176(27)	0.4479(19)	0.0828(25)	0.0070(25)
O(4)	0.1844(27)	0.4388(19)	0.4257(25)	0.0070(25)
O(5)	0.1199(28)	0.7982(18)	0.6143(27)	0.0070(25)
573 K				
Ca	0.9930(11)	0.6693(7)	0.2600(11)	0.0039(22)
Ge(1)	0.9969(7)	0.3135(4)	0.2465(7)	0.0048(14)
Ge(2)	0.0	0.0	0.0	0.0051(20)
Ge(3)	0.0	0.0	0.5	0.0056(20)
O(1)	0.9979(32)	0.9266(17)	0.2499(28)	0.0097(25)
O(2)	0.4009(29)	0.2929(19)	0.9021(27)	0.0097(25)
O(3)	0.8169(27)	0.4452(20)	0.0841(26)	0.0097(25)
O(4)	0.1877(27)	0.4377(19)	0.4266(26)	0.0097(25)
O(5)	0.1211(29)	0.7973(20)	0.6139(28)	0.0097(25)
648$_c$ K				
Ca	0.9976(14)	0.6698(7)	0.2583(13)	0.0096(24)
Ge(1)	0.9991(8)	0.3143(5)	0.2481(8)	0.0100(15)
Ge(2)	0.0	0.0	0.0	0.0058(21)
Ge(3)	0.0	0.0	0.5	0.0051(21)
O(1)	0.0087(37)	0.9286(16)	0.2547(31)	0.0052(25)
O(2)	0.3952(32)	0.2928(19)	0.9046(29)	0.0052(25)
O(3)	0.8096(29)	0.4421(20)	0.0778(28)	0.0052(25)
O(4)	0.1830(29)	0.4358(20)	0.4216(27)	0.0052(25)
O(5)	0.1116(32)	0.7990(20)	0.6063(31)	0.0052(25)
673 K				
Ca	0.9978(14)	0.6700(7)	0.2538(13)	0.0063(22)
Ge(1)	0.9998(8)	0.3143(4)	0.2467(9)	0.0080(14)
Ge(2)	0.0	0.0	0.0	0.0068(20)
Ge(3)	0.0	0.0	0.5	0.0063(20)
O(1)	0.0092(36)	0.9276(16)	0.2487(32)	0.0054(23)
O(2)	0.3984(31)	0.2966(19)	0.9061(28)	0.0054(23)
O(3)	0.8161(29)	0.4403(20)	0.0805(28)	0.0054(23)
O(4)	0.1843(29)	0.4379(20)	0.4222(27)	0.0054(23)
O(5)	0.1181(31)	0.7992(20)	0.6063(30)	0.0054(23)
673$_c$ K				
Ca	0.9991(15)	0.6698(7)	0.2580(14)	0.0123(23)
Ge(1)	0.9999(9)	0.3144(4)	0.2486(9)	0.0093(14)
Ge(2)	0.0	0.0	0.0	0.0069(21)
Ge(3)	0.0	0.0	0.5	0.0041(21)
O(1)	0.0069(40)	0.9273(16)	0.2487(33)	0.0042(23)
O(2)	0.3949(33)	0.2940(19)	0.9021(29)	0.0042(23)
O(3)	0.8141(30)	0.4404(21)	0.0783(29)	0.0042(23)
O(4)	0.1848(30)	0.4396(21)	0.4250(28)	0.0042(23)
O(5)	0.1173(33)	0.7980(20)	0.6074(31)	0.0042(23)
703$_c$ K				
Ca	0.9985(17)	0.6698(6)	0.2539(14)	0.0120(19)
Ge(1)	0.9993(10)	0.3138(4)	0.2498(9)	0.0079(12)
Ge(2)	0.0	0.0	0.0	0.0044(20)
Ge(3)	0.0	0.0	0.5	0.0091(22)
O(1)	0.9989(44)	0.9269(14)	0.2541(35)	0.0050(20)
O(2)	0.3957(34)	0.2972(20)	0.9026(30)	0.0050(20)
O(3)	0.8159(32)	0.4441(22)	0.0816(29)	0.0050(20)
O(4)	0.1858(32)	0.4345(22)	0.4286(28)	0.0050(20)
O(5)	0.1192(35)	0.7999(20)	0.6079(31)	0.0050(20)
723 K				
Ca	0.0035(19)	0.6696(5)	0.2524(17)	0.0060(16)
Ge(1)	0.9991(12)	0.3140(3)	0.2473(10)	0.0070(10)
Ge(2)	0.0	0.0	0.0	0.0030(22)
Ge(3)	0.0	0.0	0.5	0.0122(24)
O(1)	0.993(5)	0.9268(13)	0.2456(42)	0.0100(19)
O(2)	0.391(4)	0.2985(23)	0.8984(35)	0.0100(19)
O(3)	0.815(4)	0.4383(25)	0.0803(33)	0.0100(19)
O(4)	0.185(4)	0.4394(25)	0.4273(32)	0.0100(19)
O(5)	0.114(4)	0.7958(22)	0.6010(36)	0.0100(19)
723$_c$ K				
Ca	0.9999(18)	0.6697(5)	0.2530(17)	0.0090(16)
Ge(1)	0.9985(11)	0.3144(31)	0.2480(10)	0.0081(10)
Ge(2)	0.0	0.0	0.0	0.0056(22)
Ge(3)	0.0	0.0	0.5	0.0083(23)
O(1)	0.990(5)	0.9250(13)	0.2463(40)	0.0044(18)
O(2)	0.383(4)	0.2975(22)	0.9045(33)	0.0044(18)
O(3)	0.822(4)	0.4412(24)	0.0849(30)	0.0044(18)
O(4)	0.194(4)	0.4345(24)	0.4314(30)	0.0044(18)
O(5)	0.107(4)	0.7960(22)	0.6068(34)	0.0044(18)
748 K				
Ca	0.0	0.6695(5)	0.25	0.0128(17)
Ge(1)	0.0	0.31398(32)	0.25	0.0079(10)
Ge(2)	0.0	0.0	0.0	0.0089(9)
O(1)	0.0	0.9260(14)	0.25	0.0145(45)
O(2)	0.1849(13)	0.4386(9)	0.4231(14)	0.0107(31)
O(3)	0.1125(14)	0.7974(9)	0.6029(14)	0.0074(29)
748$_c$ K				
Ca	0.0	0.6693(5)	0.25	0.0127(17)
Ge(1)	0.0	0.31372(32)	0.25	0.0080(10)
Ge(2)	0.0	0.0	0.00	0.0087(9)
O(1)	0.0	0.9251(14)	0.250000	0.0134(45)
O(2)	0.1860(13)	0.4383(9)	0.4259(13)	0.0048(30)
O(3)	0.1092(14)	0.7961(9)	0.5988(14)	0.0047(29)
773 K				
Ca	0.0	0.6696(5)	0.25	0.0114(16)
Ge(1)	0.0	0.31380(31)	0.25	0.0092(10)
Ge(2)	0.0	0.0	0.0	0.0088(9)
O(1)	0.0	0.9282(13)	0.25	0.0115(42)
O(2)	0.1839(12)	0.4398(9)	0.4223(13)	0.0093(29)
O(3)	0.1133(13)	0.7975(9)	0.6027(14)	0.0064(28)
798 K				
Ca	0.0	0.6691(5)	0.25	0.0163(16)
Ge(1)	0.0	0.3138(3)	0.25	0.0076(10)
Ge(2)	0.0	0.0	0.0	0.0091(9)
O(1)	0.0	0.9272(13)	0.25	0.0147(43)
O(2)	0.1826(13)	0.4405(9)	0.4219(13)	0.0127(30)
O(3)	0.1097(13)	0.7983(9)	0.6021(14)	0.0052(28)

Table 2 (Contd.)

293 K	x	y	z	U_{iso} (Å^2)
823 K				
Ca	0.0	0.6704(5)	0.25	0.0124(15)
Ge(1)	0.0	0.3140(3)	0.25	0.0091(10)
Ge(2)	0.0	0.0	0.0	0.0093(8)
O(1)	0.0	0.9264(13)	0.25	0.0188(45)
O(2)	0.1878(12)	0.4372(8)	0.4253(13)	0.0038(28)
O(3)	0.1105(13)	0.7962(9)	0.6022(14)	0.0091(28)
823c K				
Ca	0.0	0.6697(5)	0.25	0.0123(16)
Ge(1)	0.0	0.3142(3)	0.25	0.0064(10)
Ge(2)	0.0	0.0	0.0	0.0081(9)
O(1)	0.0	0.9252(13)	0.25	0.0132(44)
O(2)	0.1847(13)	0.4394(9)	0.4220(14)	0.0080(30)
O(3)	0.1092(14)	0.7968(9)	0.6034(15)	0.0129(30)
873$_c$ K				
Ca	0.0	0.6691(5)	0.25	0.0158(16)
Ge(1)	0.0	0.3140(3)	0.25	0.0089(10)
Ge(2)	0.0	0.0	0.0	0.0098(9)
O(1)	0.0	0.9257(13)	0.25	0.0126(42)
O(2)	0.1847(12)	0.4385(8)	0.4257(13)	0.0081(29)
O(3)	0.1139(13)	0.7980(9)	0.6019(13)	0.0040(27)
923 K				
Ca	0.0	0.6703(5)	0.25	0.0161(16)
Ge(1)	0.0	0.3139(3)	0.25	0.0086(10)
Ge(2)	0.0	0.0	0.0	0.0096(9)
O(1)	0.0	0.9287(12)	0.25	0.0105(41)
O(2)	0.1865(12)	0.4387(9)	0.4245(13)	0.0161(31)
O(3)	0.1117(13)	0.7971(9)	0.6025(14)	0.0115(28)

Results and discussion

The $C\bar{1} \leftrightarrow C2/c$ phase transition

Clear evidence of the triclinic-monoclinic transition is seen in the lattice parameters as a function of temperature (Fig. 2), whereas the heat capacity data show only a weak and broad anomaly near 700 K (Fig. 1).

Deviation from the calculated intensity based on the triclinic structure model is found between several reflections hkl and $h\bar{k}l$, which are rendered symmetry-inequivalent by the transition to the triclinic phase. The strongest such deviation occurs between the 130 and 1$\bar{3}$0 reflection, as is demonstrated in Fig. 3. The origin of these deviations is not clear, but it might be due to structural modulations that cannot be resolved using the presently available data.

In order to calculate the components of the spontaneous strain tensor in the triclinic phase, the thermal expansion has to be estimated from the behaviour above the critical temperature. These extrapolations are shown in Fig. 2. The deviations from the extrapolated thermal expansion are small along [100] and [010], and nearly absent along [001]. A volume strain of about −0.11% is observable at room temperature (Fig. 2c). Lattice strain as a result of the phase transition is most obvious from the temperature evolution of the angles α, β and γ. The deviation from 90° is strongest for α at ambient temperature, where it amounts to about 2%. The components of the spontaneous strain tensor were calculated using the equations given by Carpenter et al. (1998). Their values are plotted against temperature in Fig. 4. The non-symmetry-breaking (nsb) strains e_{11}, e_{22}, e_{33} and e_{13} are smaller than the two symmetry-breaking strains e_{23} and e_{12} by 1 order of magnitude. We will thus neglect the nsb strain components in the following analysis.

As a result of the phase transition, the position of the Ca atom shifts away from the diad axis of the monoclinic phase. This displacement occurs entirely within the (**a**, **c**) plane or normal to **b***. The direction of the displacement is approximately parallel [102] or **c***. Figure 5 shows that the Ca displacement is a linear function of the symmetry-breaking strain components. If we take the symmetry-breaking strain $e_4 = 2e_{23}$ to be the driving order parameter of the transition (*cf. the discussion of albite by Carpenter and Salje* 1998), with $e_6 = 2e_{12}$ linearly coupled to it, the free energy can be expanded as:

$$G' = \frac{1}{2}a'(T - T_c)e_4^2 + \frac{1}{4}b'e_4^4 + C_{46}^0 e_4 e_6 + \frac{1}{2}C_{66}^0 e_6^2 \ . \qquad (1)$$

C_{46}^0 and C_{66}^0 are bare elastic constants, i.e. C_{66} and C_{46} are not supposed to vary with temperature. With a stress-free crystal under equilibrium conditions, the relation $e_6 = -C_{46}^0 e_4 / C_{66}^0$ holds, and hence Eq. (1) simplifies to:

$$G' = \frac{1}{2}a'(T - T_c^\star)e_4^2 + \frac{1}{4}b'e_4^4 \ , \qquad (2)$$

where the renormalized critical temperature is $T_c^\star = T_c + (C_{46}^0)^2/(a'C_{66}^0)$. Equation (2) is equivalent to the standard Landau polynomial for a second-order phase transition. Thus, the temperature evolution of the squared order parameter follows as

$$e_4^2 = (e_4^0)^2\left(1 - \frac{T}{T_c^\star}\right) \ , \qquad (3)$$

where $(e_4^0)^2$ is the saturation value of the squared order parameter at low temperatures. The square root of this equation (and the equivalent for e_6) has been used to approximate the temperature behaviour of e_{23} and e_{12} in Fig. 4. The renormalized critical temperature of $T_c^\star = 714 \pm 3$ K was estimated by extrapolation of the squared scalar strain, $\sum e_{ij}^2$ (Fig. 6), to zero. Two sets of data recorded above this temperature, at $T = 723$ K, still yielded significantly better R values in the triclinic setting. The parameters $e_{12}^0 = -0.0111(1)$ and $e_{23}^0 = 0.0175(1)$ result from the Landau approximation of the symmetry-breaking strain components. Thus it follows that $C_{46}^0/C_{66}^0 = -e_{12}^0/e_{23}^0 \approx 2/3$. The second derivative of Eq. (1) with respect to e_4 yields the temperature dependence of C_{44}:

$$C_{44} = a'(T - T_c) + 3b'e_4^2 \ , \qquad (4)$$

which softens to $(C_{46}^0)^2/C_{66}^0 \approx 2C_{46}^0/3$ at $T_c^\star$.

In order to adequately describe the peak profiles in the Rietveld refinements, their anisotropic broadening had to be accounted for, based on the assumption of a

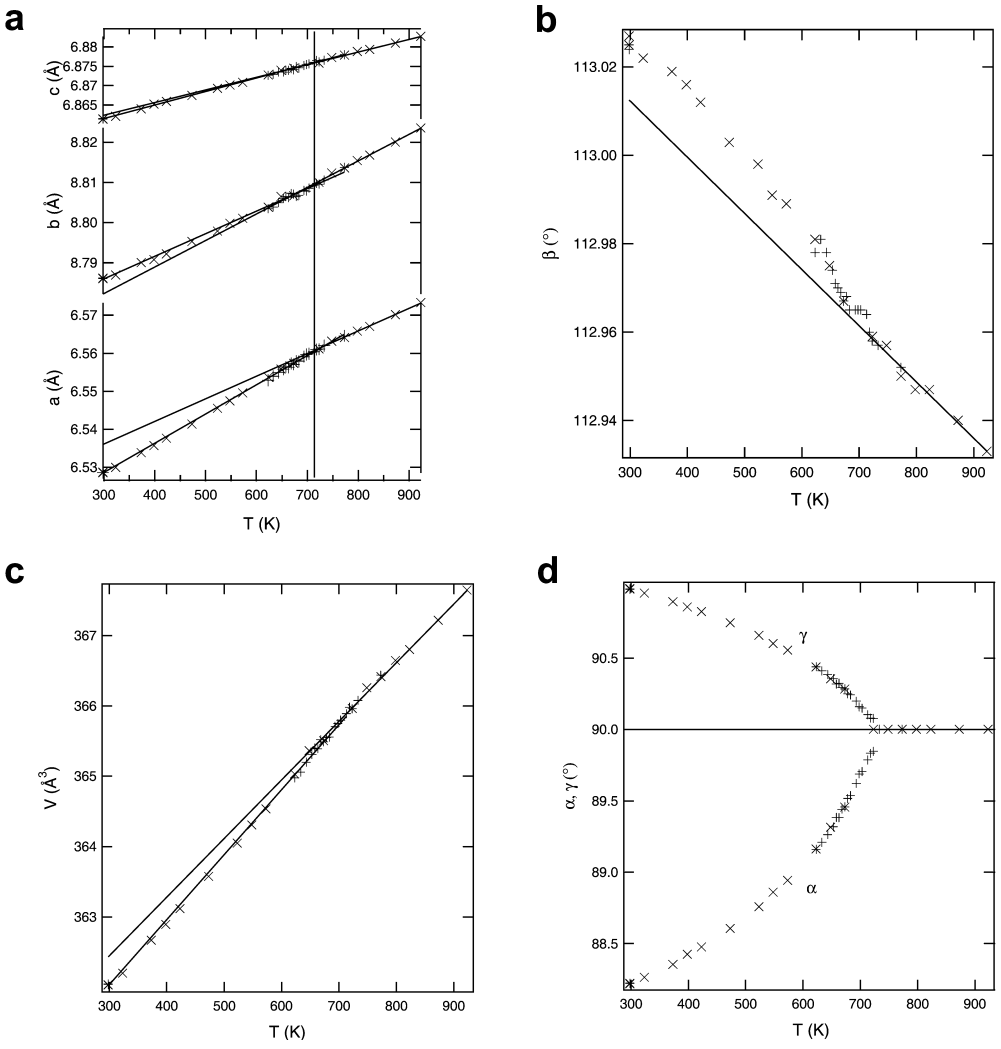

Fig. 2a–b Lattice parameters of CDG as a function of temperature. *Error bars* are of the order or smaller than the shown symbol sizes. *Symbols* + and × in this and in the following graphs mark the results obtained in two separate heating runs

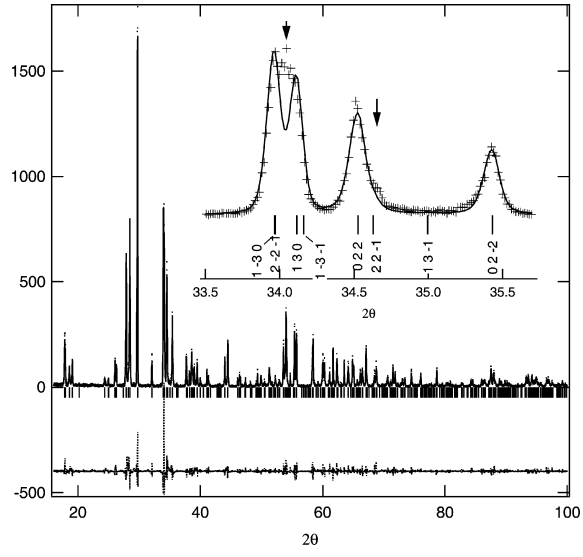

Fig. 3 Observed, calculated and difference powder diffraction intensity at room temperature. Peak positions are indicated by vertical markers. The inset shows a magnified portion of the diagram around the 130 and the 130 reflections

microstrain distribution (Stephens 1999). The parameter S_{022} dominates the anisotropic peak broadening at all temperatures. It is at least twice as large as any other of the 15 microstrain parameters allowed in the triclinic setting. The temperature evolution of S_{022} is shown in Fig. 7. As S_{022} accounts for those contributions to the variance of d^{-2} that are proportional to k^2l^2, it reflects the variance of the angle $\alpha^\star$ or a positive correlation of the magnitudes of $b^\star$ and $c^\star$. The presence of these fluctuations of the reciprocal lattice dimensions might be related to the softening of C_{44} at the phase transition.

The values of the coefficients a and b can now be determined from the calorimetric data. Figure 1 shows that the phase transition has only little effect on the heat capacity, with a barely perceptible jump occurring near 714 K. Linear extrapolation of the heat-capacity data from below and above this temperature, weighted by the esd obtained by averaging several c_p scans, yields the discontinuity in c_p at T_c^* as $\Delta c_p = 2 \pm 0.2$ J(K mol)$^{-1}$. Hence $a = 2\Delta c_p \approx 4$ J (K mol)$^{-1}$ and $b = aT_c^\star \approx 2.860$ kJmol^{-1}. Rescaling the coefficients by $(e_4^0)^2 =$

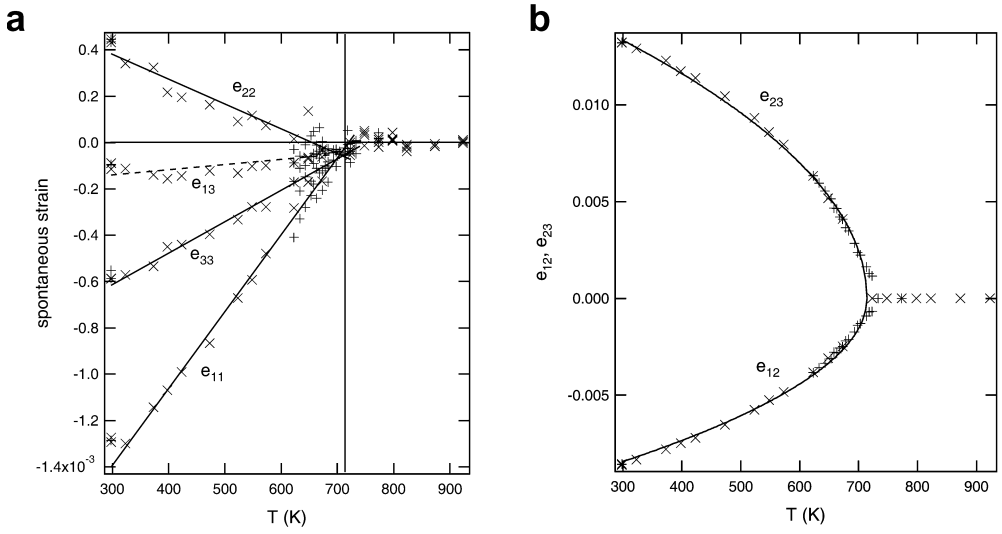

Fig. 4a b Spontaneous strain as a function of temperature. **a** shows the non-symmetry-breaking strain components and **b** shows the symmetry breaking components. The *solid curves* in **b** indicate the temperature behaviour given by the Landau model. The *straight lines* in **a** are guides to the eye

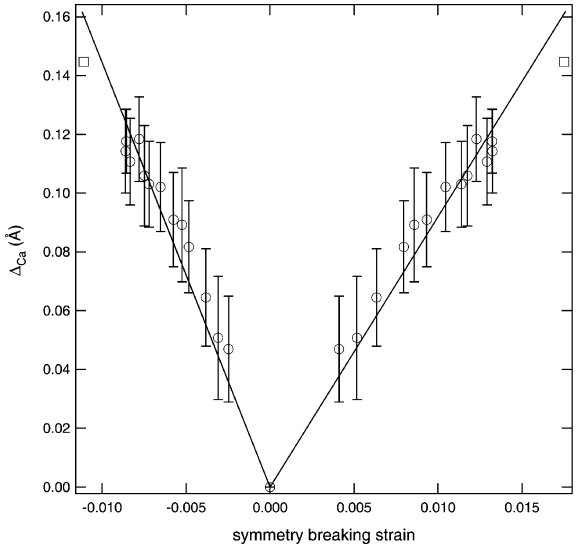

Fig. 5 Ca displacement as a function of the symmetry-breaking strain components e_{12} and e_{23}. The *square symbols* represent the displacement obtained by first-principle structure optimization plotted versus e_{12}^0 and e_{23}^0, respectively

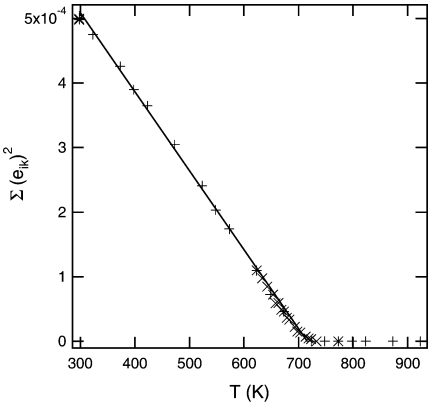

Fig. 6 Squared scalar strain as a function of temperature

0.00031 and $(e_4^0)^4 = 9.4 \times 10^{-8}$ to obtain a' and b' in Eq. (2) gives 12.9 kJ(K mol)$^{-1}$ and 30.43×10^6 kJmol^{-1} respectively.

Verification of the $C\bar{1}$ structure

Using the full potential augmented plane wave method as implemented in the Wien2k program (Blaha et al. 2001) the acentric structure model of CDG of Nevskii et al. (1979) has been optimized in space group symmetry P1. The calculations were performed using the default LAPW basis functions with muffin-tin radii chosen as 1.8, 1.7 and 1.4 a.u. for Ge, Ca and O, respectively. The exchange-correlation functional was treated in the generalized gradient approximation (GGA) (Perdew et al. 1996). States below −6.0 Ryd were treated as core electrons. The plane-wave cutoff was set to $R_{mt}k_{max} = 7$ and the basis set contained more than 2500 plane waves. Force optimization was carried

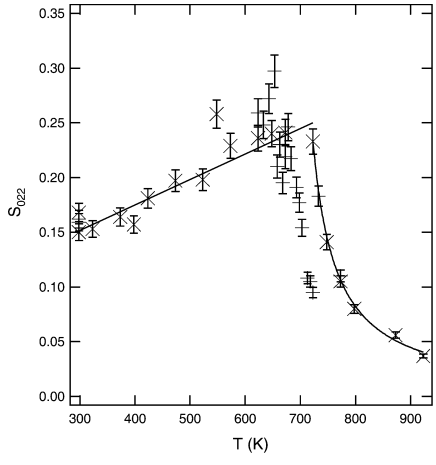

Fig. 7 Anisotropic peak broadening parameter S_{022} as a function of temperature. The *lines* are guides to the eye

Table 3 Computationally predicted atomic positions (transformed to SG setting $C\bar{1}$) and their deviation from the experimental values. *Numbers in parentheses* denote the errors of the Rietveld analysis. The lattice parameters are those given in table 1 for 293 K

	x	$x - x_o$	y	$y - y_o$	z	$z - z_o$
Ca	0.9898	−0.0012(7)	0.6696	0.0002(5)	0.2691	0.0031(7)
Ge(1)	0.9956	−0.0015(4)	0.3155	0.0013(3)	0.2423	−0.0016(4)
Ge(2)	0.0	0.0	0.0	0.0	0.0	0.0
Ge(3)	0.0	0.0	0.0	0.0	0.5	0.0
O(1)	0.0021	0.0028(20)	0.9275	−0.0003(12)	0.2545	0.0022(18)
O(2)	0.4023	−0.0010(24)	0.2932	−0.0032(12)	0.9110	0.0066(18)
O(3)	0.8098	−0.0034(18)	0.4518	0.0013(13)	0.0742	−0.0091(17)
O(4)	0.1920	0.0024(18)	0.4290	−0.0052(12)	0.4403	0.0106(17)
O(5)	0.1223	0.0035(19)	0.8027	−0.0008(12)	0.6155	0.0007(18)

out with a damped Newton scheme to a tolerance of 0.4 mRy a.u.$^{-1}$. Fifty k-points were sampled in the entire Brillouin zone, corresponding to 14 k-points in the irreducible wedge. The lattice parameters given by Nevskii et al. (1979), as well as appropriately transformed room-temperature lattice parameters of this study (Table 1), were used.

The results show that the structural parameters given by Nevskii et al. (1979) do indeed converge to a centrosymmetric structure. The final, calculated energy does not differ from the energy of an equivalent, optimized structure model in SG $P\bar{1}$. Based on the measured room-temperature lattice parameters of this study, satisfactory agreement between the computed and the experimentally observed structural parameters is obtained (Table 3). Only the z coordinates of the Ca, O(3) and O(4) atoms are outside a margin of 4 esd with respect to the results of the Rietveld structure refinements. These slight deviations are most likely due to the ground-state properties of the calculated structure and a correspondingly saturated Ca displacement. As a consequence, the Ca shift resulting from the density functional calculations approaches the linear trend in Fig. 5, when it is plotted against the respective saturation values, e^0_{12} and e^0_{23}, of the symmetry-breaking strain components.

Based on Eq. 2 and its parameter values derived from the calorimetric data the excess energy associated with the phase transition would amount to $\Delta H = -b/4 = -715 \pm 150$ Jmol^{-1}. In order to determine this energy using first-principle calculations, the reference energy of the high-symmetry phase has to be calculated. The reference state is a monoclinic structure with a cell volume identical to the $P\bar{1}$ structure calculated above. In order to obtain the correct lattice parameters the extrapolated values a_0, b_0, c_0 and β_0 (Fig. 2) of the hypothetical monoclinic structure at room temperature have to be corrected for the nsb strain that was neglected in the Landau approximation. This is accomplished by using lattice parameters $a_m = (e_{11} + 1)a_0 = 6.5276$ Å, $b_m = (e_{22} + 1)b_0 = 8.786$ Å, $c \approx c_0 = 6.8623$ Å. Based on the cell volume at room temperature (Table 1) the corresponding monoclinic angle is $\beta = 113.09°$. This cell with the atomic positions determined at T = 748 K (Table 3) is then transformed to the primitive, non-conventional setting (a = b = 5.47274 Å, c = 6.8623 Å, $\alpha = \beta = 103.525°$, $\gamma = 106.779°$). Force minimization using Wien2k and the conditions previously stated yields an excess energy $\Delta U = 670$ J mol^{-1} with respect to the $P\bar{1}$ structure given in Table 3. This value compares well with the energy estimated using the Landau approximation.

Conclusions

The triclinic to monoclinic phase transition in $CaGe_2O_5$ occurs near 714 K. The transition displays classical second-order behaviour with the symmetry-breaking strain as the order parameter. Microscopically, the order parameter is identified with the displacement of the Ca atom. Analysis of the microstrain broadening of the powder peak profiles provides additional evidence of the phase transition. The sharp increase of this microstrain broadening on approaching the phase transition from high temperatures possibly is related to the softening of the C_{44} elastic constant. Based on these results CDG constitutes a ferroelastic material.

Acknowledgements We would like to thank L. Cemič for his support at the Institut für Geowissenschaften in Kiel. R. Angel is thanked for helpful discussions on the subject. The work was funded by Deutsche Forschungsgemeinschaft.

References

Angel RJ (1997) Transformation of fivefold-coordinated silicon to octahedral silicon in calcium silicate, $CaSi_2O_5$. Am Mineral 82: 836–839

Angel RJ, Ross NL, Seifert F, Fliervoet TF (1996) Structural characterization of pentacoordinate silicon in a calcium silicate. Nature 384: 441–444

Aust H, Völlenkle H, Wittmann A (1976) Die Kristallstruktur der Hoch- und der Tieftemperaturform von $CaGe_2O_5$. Z Kristallogr 144:82–90

Blaha P, Schwarz K, Madsen GKH, Kvasnicka D, Luitz J (2001) WIEN2k, an augmented plane wave + local orbitals program for calculating crystal properties. Karlheinz Schwarz, Techn. Universität Wien, Austria. ISBN 3-9501031-1-2

Bosenick A, Geiger CA, Cemič L (1996) Heat-capacity measurements of synthetic pyrope-grossular garnets between 320 and 1000 K by differential scanning calorimetry. Geoch Cosmoch Acta 60: 3215–3227

Cammenga HK, Eysel W, Gmelin W, Hemminger W, Höhne WGH, Sarge SM (1992) Die Temperaturkalibrierung dynami-

scher Kalorimeter II. Kalibriersubstanzen. PTB Mitteilungen 102: 13–18

Carpenter MA, Salje EKH (1998) Elastic anomalies in minerals due to structural phase transitions. Eur J Mineral 10: 693–812

Carpenter MA, Salje EKH, Graeme-Barber A (1998) Spontaneous strain as a determinant of thermodynamic properties for phase transitions in minerals. Eur J Mineral 10: 621–691

Ditmars DA, Douglas TB (1971) Measurements of the relative enthalpy of pure α-Al_2O_3 (NBS heat capacity and enthalpy reference material no. 720) from 273 to 1173 K. J Res NBS (A) Phys Chem 75: 401–420

Finger LW, Cox DE, Jephcoat AP (1994) A correction for powder diffraction peak asymmetry due to axial divergence. J Appl Crystallogr 27: 892–900

Groat LA, Raudsepp M, Hawthorne FC, Ercit TS, Sherriff BL, Hartman JS (1990) The amblygonite–montebrasite series: characterization by single-crystal structure refinement, infrared spectroscopy, and multinuclear MAS-NMR spectroscopy. Am Mineral 75: 992–1008

Larson A, Von Dreele R (1994) General structure analysis system (GSAS). Tech Rep LAUR B6-748, Los Alamos National Laboratory Report, Los Alamos, New Mexico

McAdie HG, Garn PD, Menis O (1972) Standard reference materials: selection of differential scanning analysis temperature standards through a cooperative study. NBS, Special Publication: 260-40. SRM 758, 759, 760

Mongiorgi R, Riva di Sanseverino L (1968) A reconsideration of the structure of titanite, $CaTiOSiO_4$. Miner Petrogr Acta 14: 123–141

Mraw SC (1988) Differential scanning calorimetry. In: Ho CY (ed), Data series on material properties, vols. 1–2, chap 11 pp 395–437

Nevskii NN, Ilyukhin VV, Belov NV (1979) The crystal structure of $CaGe_2O_5$ – a germanium analog of sphene. Sov Phys Dokl 24: 415–416

Perdew JP, Burke S, Ernzerhof M (1996) Generalized gradient approximation made simple. Phys Rev Lett 77: 3865–3868

Stephens PW (1999) Phenomenological model of anisotropic peak broadening in powder diffraction. J Appl Crystallogr 32: 281–289

Taylor M, Brown G (1976) High-temperature structural study of the $P2_1/a \leftrightarrow A2/a$ phase transition in synthetic titanite, $CaTiSiO_5$. Am Mineral 61: 435–447